Structural Analysis of a Cooled, Directionally Solidified Turbine Blade

E. E. Abell,* R. E. Kielb,† and P. J. Henderson‡
Aeronautical Systems Division, Wright-Patterson Air Force Base, Ohio

Directionally solidifed, air-cooled turbine blades present new challenges to the structural design analyst. This paper describes an investigation of turbine blade failures encountered during a recent engine development program. The effect of wall tolerance variations on steady and vibratory stresses was determined using finite-element methods (NASTRAN) combined with engine test data. This procedure successfully determined the failure mechanism and verified the subsequent redesign.

Introduction

PAST design practices for aircraft engine turbine blades have concentrated on simplified theories and limited analysis. Most designs have been based on an extrapolation of previous successful hardware using these simplified techniques. The basic approach has been to approach the blade as a beam with distributed pressure loads due to aerodynamic forces. The airfoil stresses due to pressure loads and airfoil tilt are calculated using classical beam theory. By the method of superposition, centrifugally and thermally induced stresses are added to the blade to arrive at the total stress field. Critical locations then are defined for both creep and stress rupture calculations using standard procedures. These stresses also were used to determine projected low cycle fatigue lives and the vibratory allowables.

The drive to higher performance machines has resulted in several advances in blade technology. These advances have reduced the effectiveness of the classical techniques in analyzing the blade to insure satisfactory operation. Key among these advances has been directional solidification[1] (DS) of blade alloys and highly complex airfoil cooling schemes. The first of these items leads to a very complex generalized Hooke's Law relationship, which cannot be handled easily with classical methods. The advanced cooling arrangements used in modern engines result in complex load paths and severe temperature gradients that make the planes-remain-plane bending assumption questionable.

Heavy emphasis is placed on increasingly expansive engine tests to verify these calculations. Although it offers the only complete answer to the proof of the design, the need to drive development cost lower has reduced available test time. To make optimum usage of this test time, more accurate stress/strain analyses are needed to 1) interpret, interpolate, and extrapolate test results; 2) obtain data on immeasurable parameters; and 3) reduce iterations through the design/test/redesign cycle.

The finite-element method of structural analysis provides the opportunity to perform a more accurate analysis of complex structures such as cooled turbine blades. This paper presents an example of how the finite-element method was used to explain failures, provide data for a redesign, and analyze the redesign to determine its failure susceptibility of a DS, cooled, turbine blade.

Presented at the AIAA/ASME/SAE 17th Structures, Structural Dynamics, and Materials Conference, King of Prussia, Pa., May 5–7, 1976 (no preprints, bound volume pp. 291-297); submitted May 19, 1976; revision received Aug. 9, 1976.

Index categories: Airbreathing Propulsion, Subsonic and Supersonic; Structural Static Analysis.

*Technical Specialist. Member AIAA.
†Aerospace Engineer.
‡Aerospace Engineer. Member AIAA.

Problem Description

The specific blade considered in this study is shown in Fig. 1. There are 72 identical blades in the turbine stage. The blade has a two-tooth attachment, a rectangular hollow extended neck, a forward and rear buttress, a platform, and a hollow airfoil. The cooling air enters two holes in the bottom of the attachment and exits through the tip of the airfoil. There are 74 pins (0.049 o.d.) connecting the pressure (concave) and suc-

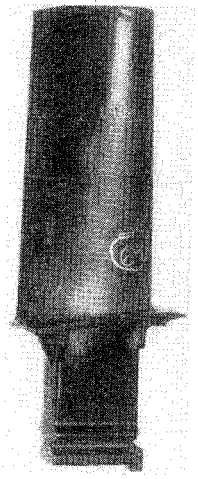

Fig. 1 Cooled, DS, turbine blade (convex side).

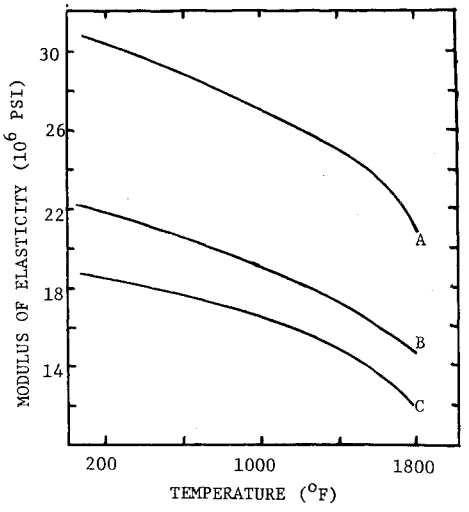

Fig. 2 Modulus of elasticity as a function of temperature for (A) conventionally cast and for directionally solidifed blade in the (B) transverse and (C) longitudinal directions.

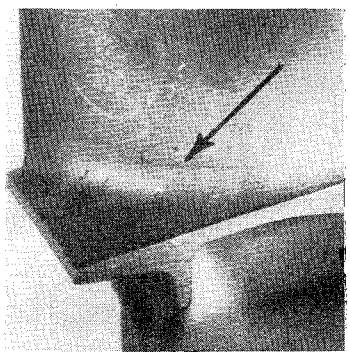

Fig. 3 Typical crack location.

tion (convex) sides of the airfoil. In addition, there are 14 pins in the extended neck. The blade is made from a DS casting of a nickel-base superalloy. This process improves the materials stress rupture properties in the spanwise direction; however, it also makes the elastic properties anisotropic. As can be seen in Fig. 2, the directionality of material properties has a significant effect on the respective spanwise and chordwise elastic moduli.

This blade had performed well in development testing and the early stages of production. It was during production acceptance testing that a small percentage of blades was found to be cracked or separated. As a result, a comprehensive effort was undertaken to determine the failure mechanism and find a solution. The initiation point for the cracks was in the root at approximately 50% of the chord on the suction side. A typical crack is shown in Fig. 3. Metallurgical examination showed that only one of the cracks found was a result of casting defect. The remainder were determined to be caused by fatigue. Since most of the failed blades had short periods of engine time ($\simeq$ 3 hr), a small number of engine power excursions, and metallurgical examination showed fatigue-type beach and river marking, the problem was diagnosed to be a result of a dynamic excitation leading to high cycle fatigue. The efforts to define the failure mechanism consisted of 1) analytical efforts to determine a) steady stresses, b) natural frequencies, c) normalized vibratory stresses, and d) stage vibration analyses; and 2) experimental tests to determine a) spin pit steady stress, b) blade nonrotating natural frequency, c) material fatigue properties, and d) vibratory stress during engine operation. This paper will discuss the details of the steady stress calculations and spin pit measurements.

Blade Modeling

As previously mentioned, the complexities of geometry, material properties, thermal environment, and loading conditions invalidate the traditional analysis techniques. It was concluded that a finite-element technique would be required to provide the desired accuracy. In choosing the finite-element program to use in this case, the following constraints existed: 1) large element and grid capacity, 2) anisotropic material properties, 3) material property temperature dependency, 4) plate and bar elements in library, and 5) steady-state and normal mode capabilities.

The first requirement was based on previous experience concerning the number of degrees of freedom (DOF) required for accuracy. The DS material properties force the second requirement. The third is due to the variation of material properties in the temperature range encountered. Prior experience also had shown plate elements with membrane and bending properties to give excellent results for a relatively small number of DOF's when applied to airfoils.[2,3] The presence of pins connecting the pressure and section sides of the airfoil would require bar elements. A desire not only to calculate the steady-state displacements and stresses but also to extract eigenvalues and the corresponding eigenvectors is implied in the fifth requirement.

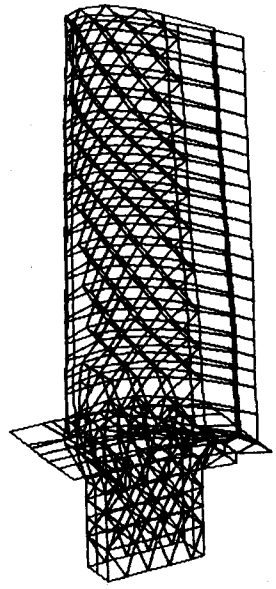

Fig. 4 Finite-element model.

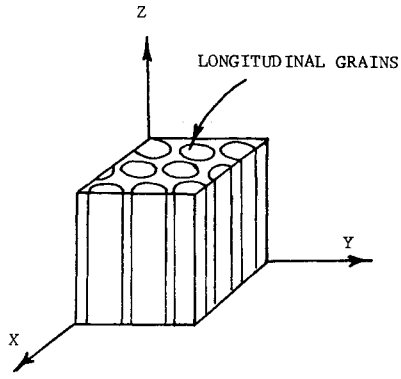

Fig. 5 Description of materials axes.

NASTRAN[4] was selected because it met these requirements and has the additional benefit of being widely used and accepted by academic, industrial, and government analysts. The NASTRAN input preparation required five steps: 1) modeling, 2) material properties, 3) temperatures, 4) loads, and 5) boundary conditions. Each of these steps will be discussed in the following paragraphs.

Since the cracks had been initiating in the root of the blade, it was desired to model the airfoil-platform intersection carefully. To have a correct simulation of the load path that transfers the airfoil centrifugal force to the attachment region, the blade was modeled completely down to the top of the first attachment tooth. Another constraint on the form of the model was the location of the pins. The arrangement of these pins suggested a triangular element pattern. With these thoughts in mind, utility programs[5,6] were used to automate the grid and element card generation. The result is shown in Fig. 4. The model consisted of 506 grid points, 761 elements, and 2713 unconstrainted DOF's.

As can be seen in Fig. 4, there appears to be a discontinuity at the junction of the pressure side and suction sides near the trailing edge. Functional constraints (NASTRAN multipoint constraints)[7] have been utilized in the process of connecting to appropriate DOF's. This has the effect of merging the suction and pressure sides into the solid trailing edge.

The final part of the modeling step was the generation of plate thickness cards. Since the failures had been statistical in nature, it was desired to identify the cause of the variance. One suspect was the blade-to-blade variation of wall thickness. Three sets of thickness cards were generated. The nominal thicknesses were used for the baseline calculations.

The other two were chosen such that the maximum and minimum stresses in root were simulated. For the maximum root stress, this was accomplished by using the minimum thickness in the root and the maximum thickness in the tip. The remaining sections varied linearly from the root to the tip. It is recognized that this is possible theoretically; however, it is very difficult to imagine a manufacturing anomaly that would cause such a thickness variation. The assumption made is, therefore, expected to be on the conservative side. The minimum stress condition was simulated using the opposite approach, i.e., maximum thickness root and minimum thickness tip.

As previously mentioned, the material used in this blade is a DS nickel-base superalloy. It consists of longitudinal grains grown in the spanwise direction. This causes elastic constraints that are anisotropic in nature. Wells[8] has derived the Hooke's Law relationship to be

$$\begin{bmatrix} \sigma_x \\ \sigma_z \\ \tau_{xz} \end{bmatrix} = \frac{E_l}{E_l - \nu_{xz}^2 E_t} \begin{bmatrix} E_t & \nu_{xz}E_t & 0 \\ \nu_{xz}E_t & E_l & 0 \\ 0 & 0 & \dfrac{E_l - \nu_{xz}^2 E_t}{E_l L} \end{bmatrix} \begin{bmatrix} \epsilon_x \\ \epsilon_z \\ e_{xz} \end{bmatrix}$$

where

E_l = longitudinal Young's modulus
E_t = transverse Young's modulus
L = shear modulus in planes parallel to longitudinal grains

The orientation of the materials axes is shown in Fig. 5. Of interest is the difference in the first and second Poisson's ratios

$$\nu_{xy} = 0.143,\ \nu_{xz} = \nu_{yz} = 0.391$$

These large differences, combined with the differences in longitudinal and transverse elastic moduli (Fig. 2), suggest that an isotropic analysis would not accurately simulate the Poisson contractions and the bending and torsion rigidities. The temperature dependency of material properties was handled by using the piecewise linear interpolation option in NASTRAN. The coefficients in the generalized Hooke's Law relationship and the coefficients of thermal expansion were input at temperatures of 1400°, 1600°, 1800°, 2000°, and 2200°F. To determine the effect of the DS material properties on the displacement and stresses, an analysis also was performed using isotropic material properties. These results will be discussed.

The cooling air entering the bottom of the blade is approximately 1000°F, and the hot gases impinging on the airfoil are well over 2000°F. The result is a severe radial, chordwise, and through-the-thickness temperature gradient.

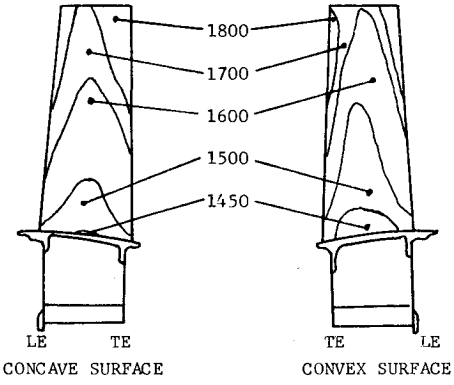

Fig. 6 Temperature contours.

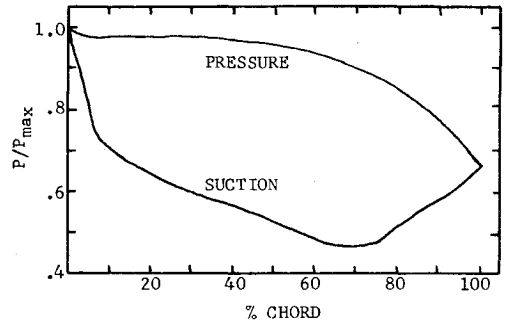

Fig. 7 Typical pressure distribution (50% span).

The temperature distribution is difficult both to calculate and to measure and, in this case, was determined by combining analytic, thermal paint, and thermocouple data. Figure 6 shows a typical temperature distribution. Figure 6 shows a typical temperature distribution. The calculation of the temperature gradient through-the-thickness showed the resulting induced thermal stresses to be small. For this reason, the radial and chordwise gradients were imposed, but the through-the-thickness gradient was ignored. NASTRAN TEMPG cards were generated for all grid points. The averaged grid temperatures are used to interpolate the material property data.

The loading conditions considered were centrifugal, thermal, and gas bending. The centrifugal loading was calculated internally by NASTRAN when given the rotational velocity vector. This was accomplished by calculating the centrifugal force for each element and distributing it among the corresponding grid points. Given the temperature and coefficient of expansion, NASTRAN calculates equivalent loads for each element to simulate the thermal expansion. Figure 7 shows a typical pressure distribution for a cross section of the airfoil. An automated process was used to integrate these distributions, subtract the internal pressure,and supply NASTRAN with elemental pressure cards. These loading conditions were put into different subcases so that the individual effects could be determined.

The grids on the lowest radial section were constrained to have zero radial displacement simulating the disk attachment. The center leading-edge point was prevented from axial diaplacement,and the pressure and suction side grids were constrained from circumferential displacement. The remaining constraints consisted of removing the rotational degrees of freedom normal to the plate elements. The axial and radial constraints were applied a distance from the area of primary interest.

Results

The first computer run was used to compare the material definition techniques. The results showed that the temperature-dependent, anisotropic material properties had a significant effect on the steady-state stress solutions. As Fig. 8

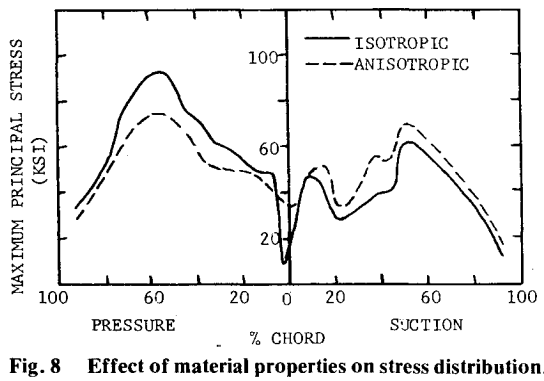

Fig. 8 Effect of material properties on stress distribution.

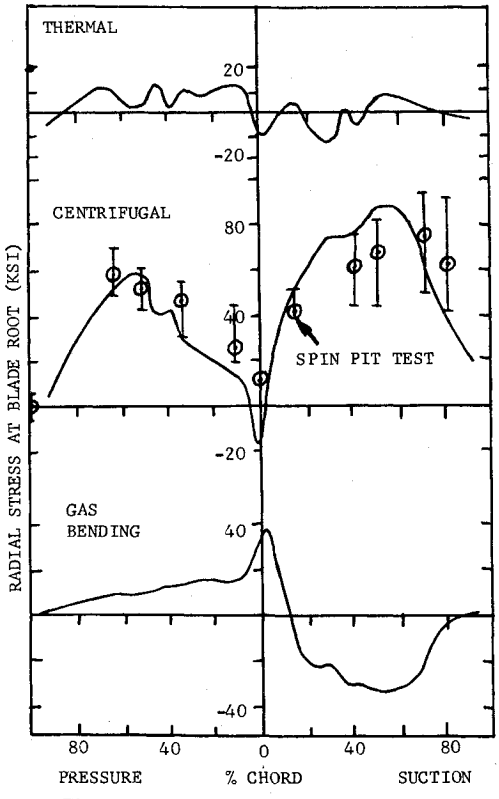

Fig. 9 Radial stress components (B/M).

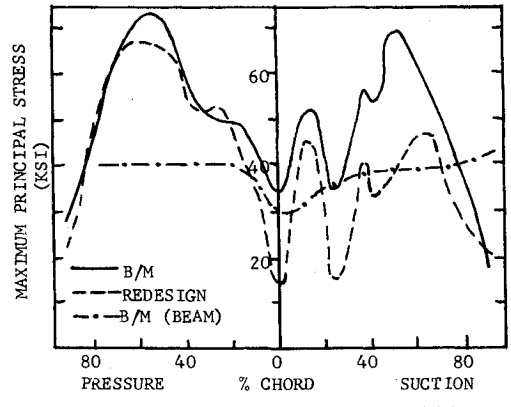

Fig. 10 Comparison of NASTRAN B/M results with beam analysis and NASTRAN redesign analysis.

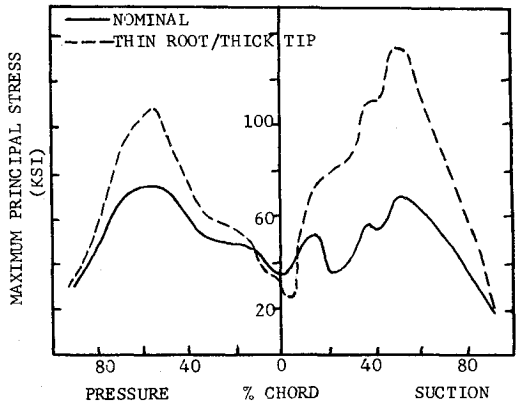

Fig. 11 Effect of airfoil wall thickness (B/M).

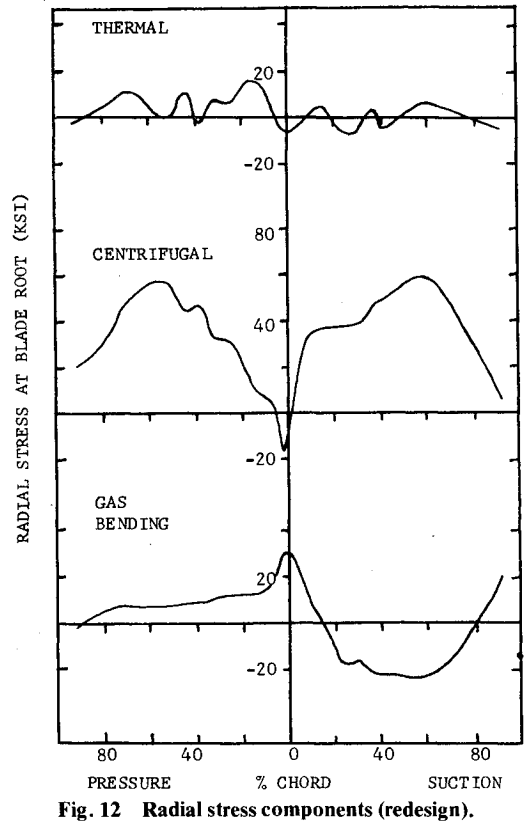

Fig. 12 Radial stress components (redesign).

shows, the anisotropic properties caused the maximum principal stress at the critical blade root area (suction side) to increase 12% over the stress of a temperature-independent, isotropic material. On the pressure side, the maximum deviation was 21%. The anisotropic material properties tended to smooth out the stress distribution. It was felt that this was due mainly to a larger shear modulus for the isotropic properties. This would have the effect of inhibiting the material's desire to distribute the radial loads evenly at the root section. All subsequent computer analyses used the anisotropic properties.

The results for the nominal wall thickness, bill-of-material (B/M) blade are shown in Fig. 9. The stresses are separated by the load components. As expected, the centrifugal stress were the most significant. The compressive stress at the leading edge ofthe airfoil base was due to a lack of support under the platform causing the leading-edge loads to seek an alternate load path to the attachment region. The stresses due to thermal loads were smaller than predicted by beam theory. This is a result of the grids going out of plane. Also shown in Fig. 9 are spin pit strain gage data. Numerous blades were tested, and the points shown are mean values with maximum and minimum bands. The spin pit is evacuated and, therefore, has no gas bending of thermal loads.

The maximum principal stress was used for comparison and evaluation of total stress at the airfoil platform intersection and is shown in Fig. 10. At some chordwise locations, the principal stress deviates significantly from the radial direction and is due to large chordwise shear stresses. The traditional analysis technique would produce an error of 42% compared to the finite-element principal stresses. Note that the principal stress on the pressure side of the bill-of-material blade is higher than that on the suction side. Later, it will be shown that the superimposed vibratory stresses are very small on the pressure side and very large on the suction side. This combined stress was the suspected cause of blade failure.

After investigating, the bill-of-material, nominal dimension blade, additional computer analyses were done to determine the effect of an unfavorable airfoil wall thickness variation (thick tip/thin root). As theorized, this combination of thicknesses, although still within drawing tolerances, could produce a steady stress (134 ksi) that would be intolerable to

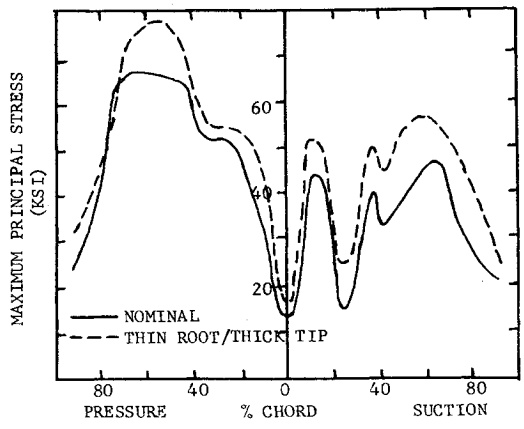

Fig. 13 Effect of airfoil wall thickness (redesign).

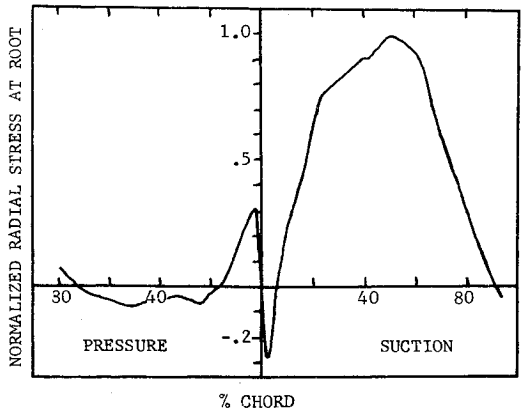

Fig. 14 Normalized vibratory stress distribution.

the blade with the vibratory stress present. As previously mentioned, this combination of tolerances, is not practically possible. However, the large scatter in measured stresses (Fig. 9) shows that wall thickness variation has a significant effect on blade steady stress. Figure 11 shows the comparison of the normal and thin-root/thick-tip principal stresses.

Blade redesign was initiated to reduce the high steady stress. Thermal stresses were small and bending stresses could not be altered significantly without an aerodynamic redesign, with potentially significant performance effects. As a result, centrifugal stress was reduced by changing the airfoil wall thickness tolerances. The wall thickness at the tip of the blade could not be reduced, since thinner walls would effect the stress-rupture life adversely. Therefore, to increase the load-carrying area, the walls were thickened at the root. This change was typically from 0.055 to 0.10 in. at the airfoil-platform intersection, midchord on the suction side. Figure 10 shows that a reduction in principal stress of 33% was accomplished in the critical area. The radial stresses in the root of the redesigned blade are shown in Fig. 12. A wall tolerance investigation of the redesigned blade was made using the same procedures as used on the B/M. Figure 13 shows how the stress variance was reduced by tightening the wall tolerance bands.

Instrumented engine tests showed large vibratory stresses in the blade root. Upon completion of the steady stress analysis, NASTRAN's Rigid Format 3 with the inverse power method was used to extract the lowest vibratory eigenvalue of the B/M blade. High computer times were required (1700 central processor seconds) for the number of degress of freedom of the structure. The corresponding eigenvector and stresses were computed. For convenience, the displacement was normalized to a unity lateral displacement of the tip. Absolute

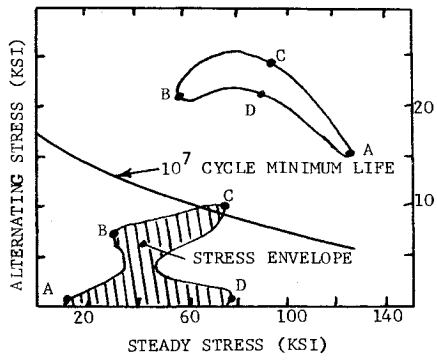

Fig. 15 Goodman diagram.

values had no meaning, since the magnitude of aerodynmic and mechanical damping was unknown. It was recognized that some reduction techniques could be used to reduce computer costs, but time did not permit further investigation.

Bench testing for natural frequencies of the blade was accomplished and compared to the NASTRAN results, showing excellent correlation (908 Hz calculated vs an average 883 Hz measured). Figure 14 shows the normalized radial stress at the root of the blade for this mode. Engine test data were then used to determine the magnitude of the vibratory stress. The lowest frequency encountered was first bending. Since the pressure side is near the neutral axis, it had a low vibratory stress. The suction side, being far from the neutral, had high vibratory stress. The steady and vibratory stresses were combined on the Goodman diagram, Fig. 15, thus demonstrating the failure mechanism.

Conclusion

The use of advanced computer codes such as NASTRAN for structural analysis of complex turbine hardware has been demonstrated successfully. The ability to handle directionally dependent material properties is a significant advantage and permits a much better representation of the true stress/strain field in the part. However, because of the criticality of boundary conditions, it often is necessary to model areas of the part not of immediate concern, such as the shank or blade neck in this case. To increase the accuracy of structural analyses, improved measurement techniques for the part environment, i.e., pressure and temperture fields, must be developed to better define the boundary conditions and loading.

The analysis performed on this blade clearly identified both the reason and the area of failure. The simplified classical techniques were inadequate to predict the potential failure in that they did not provide sufficient accuracy to determine vibratory stress margins. Also, the anisotropic properties were shown to have a significant effect on the predicted stresses. Once the model was defined sufficiently for the bill-of-material blade, checking of the proposed redesign was a simple matter of making minor changes.

The information from both the steady-state and vibratory runs permitted a much more effective use of expensive test resources. The ability to accurately extrapolate vibratory stress levels from measured locations to other areas of interest is the key to successful turbine engine airfoil design. It is necessary to use the finite-element approach to insure that proper gradients and distributions are determined so that the critical areas are defined.

A final comment is appropriate regarding the investigation of wall thickness in this paper. Too often, tolerance bands are set up based solely on manufacturing requirements. With a model such as described in this paper, it is easy and cheap to investigate the effects of such tolerance on blade capability. Only when such information is available can a rational balance between design requirements and production cost be made.

Acknowledgment

The cooperation of Pratt & Whitney Aircraft's Florida Research and Development Center (FRDC) made possible the comparison of the analytical results to experimental test data. Actual measurements were made at their facilities.

F. Gillette, E. Bryan, W. Creslein, and others of the FRDC analytical design department were extremely helpful in this investigation. Their cooperation is gratefully acknowledged.

References

[1]Sims, C. T. and Hagel, W. C. (eds.), *The Superalloys*, Wiley, New York, 1972.

[2]Allen, J. M. and Erickson, L. B., "NASTRAN Analysis of a Turbine Blade and Comparison with Field Data," ASME Paper 75-GT-77, March 1975.

[3]Anderson, D. A., "Modeling of Gas Turbine Engine Compressor Blades for Vibration Analysis," *Journal of Aircraft*, Vol. 12, April 1975, pp. 357-359.

[4]McCormick, C. W., "The NASTRAN User's Manual," NASA SP-222 (01), 1972.

[5]Ewing, M. S. and Ogg, J. S., "An Interactive Graphics Program for Mesh Creation," Aeronautical Systems Div. Wright-Patterson Air Force Base, Ohio, ENJES-TM-75-23, Sept. 1975.

[6]Kielb, R. E., "EZPLOT – A NASTRAN Aid for Plotting Undeformed Structures," Aeronautical Systems Div. Wright-Patterson Air Force Base, Ohio. ENJES-TM-75-24, Sept. 1975.

[7]MacNeal, R. H. "The NASTRAN Theoretical Manual," NASA SP-221 (01), April 1972, pp. 5.4-2-5.4-4.

[8]Wells, C. H. "The Elastic Constants of a Directionally-Solidifed, Nickel-Base Superalloy, Mar M-200," *ASM Transactions Quarterly*, Vol. 60, June 1967, pp.270-271.